Spatial mapping of the seismic vulnerability index in Kathmandu Valley: insight from dominant frequency and amplification factor

Dibyashree Poudyal [iD][1,*], **Norhaiza Nordin**[1]**, Siti Nur Aliaa Roslan**[2] **and Bhim Kumar Dahal**[3]

[1] Department of Civil Engineering, Infrastructure University Kuala Lumpur, De Centrum City, Jalan Ikram-Uniten, 43000 Kajang, Selangor, Malaysia

[2] Department of Civil Engineering, Universiti Putra Malaysia, 43400 Serdang, Selangor, Malaysia

[3] Department of Civil Engineering, Pulchowk Campus, IOE, Tribhuvan University, Lalitpur, Bagmati 44700, Nepal

*Corresponding author. Department of Civil Engineering, Infrastructure University Kuala Lumpur (IUKL), Malaysia, 43000 Kajang, Selangor Darul Ehsan, Malaysia. E-mail: 082101900007@s.iukl.edu.my

Abstract

Kathmandu Valley situated in Nepal has experienced several earthquakes in the past. The expanding population of Kathmandu Valley is driving a significant acceleration in building construction reaching record levels and posing risks to both human lives and the economy, despite this surge in development. This study aimed to spatially map the dominant frequency, amplification factor, and vulnerability index map of Kathmandu Valley, Nepal using ArcGIS. This paper presents the nonlinear response analysis of 225 boreholes using the Gorkha earthquake as input motion and DEEPSOIL software for determining the amplification ratio and dominant frequency. The results revealed a range of values for dominant frequency from 0.08 to 7.65 Hz and soil amplification ratio from 0.13 to 8.14. Furthermore, the seismic vulnerability index was derived from the dominant frequency and soil amplification ratio ranging from 0.22 to 21.84. The resulting maps acquired through this study enable the decision-makers and stakeholders, to prioritize resources and implement targeted measures for enhancing seismic resilience in the region.

Keywords: dominant frequency; nonlinear response analysis; shear wave velocity; soil amplification; vulnerability index

1. Introduction

Vulnerability refers to the sensitivity of a region to the amplification of ground shaking during an earthquake because of the underlying soil layers. Seismic waves travelling through the soils encounter a rise in amplitude, which causes greater ground motion at the surface than under bedrock circumstances. Socioeconomic vulnerability was important since it made it harder for underprivileged groups to cope with and recover from the disaster. Additionally, when damage and disruption hampered rescue and relief efforts, it became clear how vulnerable essential infrastructure systems, such as hospital networks, transportation networks, and water supply systems, were. The magnitude of the earthquake will not be uniform, with damage in locations closer to the epicentre being more severe, highlighting the vulnerability of an area due to its location. Incorporating soil amplification enables precise seismic hazard estimates at particular areas such as Kathmandu Valley offering a thorough understanding of
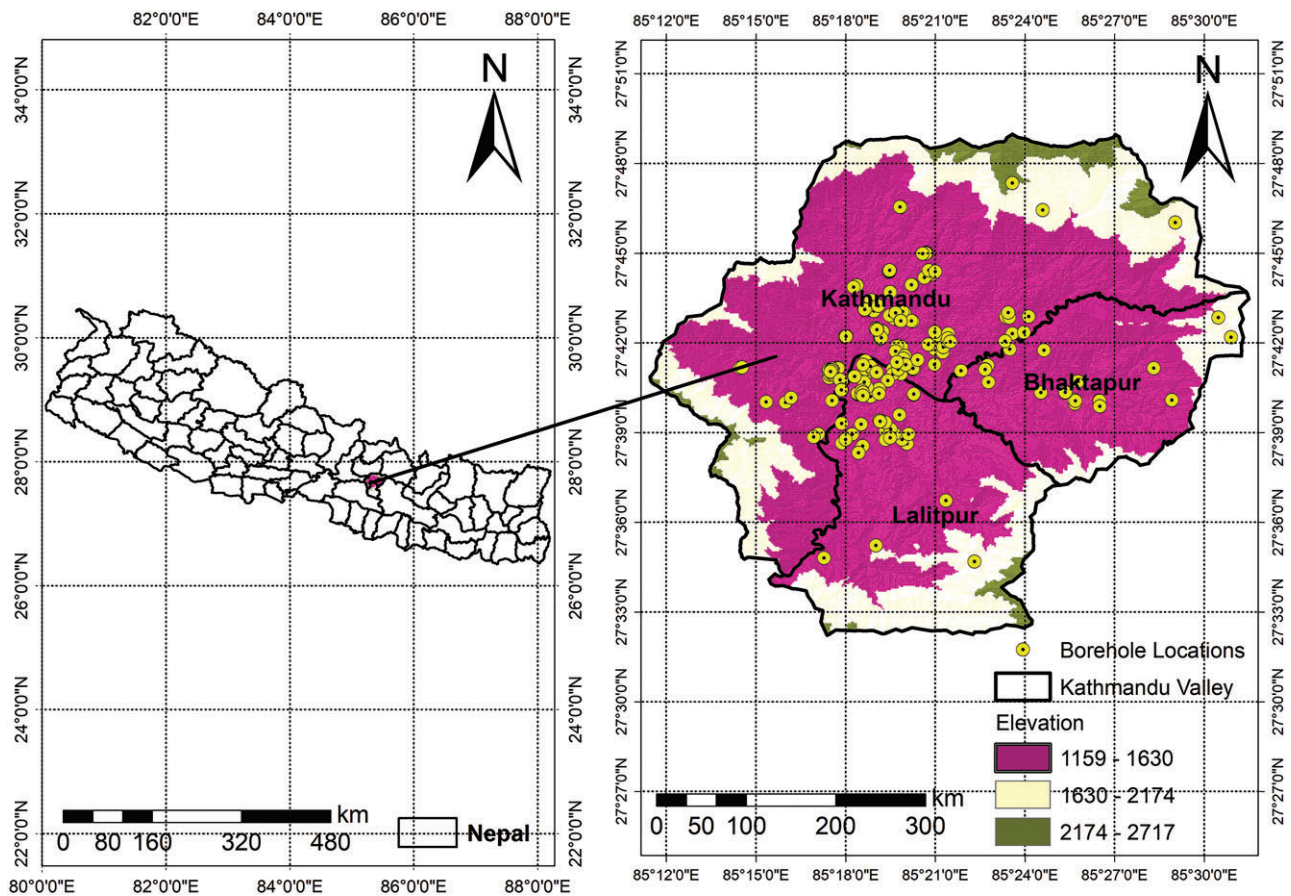
Figure 1. Study area: the Kathmandu Valley.

local seismic risks by taking into account the potential amplification of ground shaking, assisting in the identification of high-risk regions.

Throughout the history of the Kathmandu Valley, the Valley has been subjected to several powerful earthquakes. The Bhimeshwor Earthquake in 1833 (M_w 7.8), the Great Nepal-Bihar Earthquake in 1934 (M_w 8.4), the Nepal earthquake in 1988 (M_w 6.8), and the Gorkha earthquake in 2015 (M_w 7.8) are some of the most powerful earthquakes had affected the Kathmandu Valley. The 2015 Gorkha earthquake in Nepal exposed several areas of vulnerability in the impacted area. The earthquake demonstrated the vulnerability of infrastructure to structural failure, particularly in the densely populated Kathmandu Valley. Kathmandu Valley includes three historical cities, Kathmandu, Lalitpur, and Bhaktapur, located in the Bagmati province that covers an area of ~654 km². It is located between latitudes 27°24′00″N to 27°52′00″N and longitudes 85°11′00″E to 85°33′00″E as shown in Fig. 1.

The Valley is home to numerous UNESCO World Heritage Sites and many historical and cultural landmarks. However, the fast urbanization and population increase in the Valley have created problems for infrastructure planning and disaster risk reduction (Carlos *et al.* 2022). The influx of people from rural areas seeking better economic chances, health-

care facilities, educational opportunities, and other amenities is responsible for this population growth (Bhochhibhoya and Maharjan 2022). The Valley has faced several difficulties in infrastructure development and catastrophe risk management due to urbanization and the increasing population. Owing to its high seismic activity and large urban population, the vulnerability of the Kathmandu Valley has been the focus of much investigation.

Zhu *et al.* (2023) evaluated the seismic risk of Songyuan City, China by employing a system based on risk, vulnerability, and emergency response capabilities, in which GIS is used for calculating seismic hazard through the CF-logistic regression model, and vulnerability is assessed using the combined weight-TOPSIS model. Amirudin *et al.* (2023) carried out to make a map of the dominant frequency, amplification factor, seismic susceptibility index, shear wave velocity, and peak ground acceleration of coastal area of West Palu bay. Different researchers from Indonesia have carried out research related to the dominant frequency, amplification factor and vulnerability index. Their study areas are Banda Aceh City, Klaten Regency, Prambanan Temple, Batubesi Dam, and Boyolali Central Java (Mubin and Nurcahya 2014, Sunaryo 2017, Legowo *et al.* 2019, Sorja *et al.* 2019, Asnawi *et al.* 2022, respectively). Various researchers have conducted studies on

social vulnerability in different regions prone to such hazards, such as Agrawal *et al.* (2023) for the Eastern Region of India, and Mahbubur and Jerin (2022) for Bangladesh.

Gautam (2017a) disseminates district-wise social vulnerability to natural hazards in Nepal. The study conducted by Aksha *et al.* (2019) revealed that the highest levels of social vulnerability are concentrated in the central, western mountain, western hill, central, and eastern Terai regions of Nepal. The study conducted by Bhattarai and Conway (2010) examines urban vulnerabilities in five rapidly urbanizing cities in the Kathmandu Valley, Nepal, focusing on the historical context of uncontrolled urbanization, geographical features of the urban landscape, and seismic vulnerabilities. Thapa and Baral (2013) conducted a study to evaluate climate change vulnerability and its associated risks for the communities. Anhorn *et al.* (2015) investigated the urban vulnerability in Musikot, highlighting the instability in modern construction due to factors such as population growth whereas Tallett-Williams *et al.* (2016) conducted a reconnaissance mission following the 25 April 2015 (M_w 7.6) Gorkha earthquake to assess damage patterns in Nepal as well as derive shear wave velocity profiles for an individual location, which is transformed into spectral acceleration using ground motion data of the Gorkha earthquake and DEEPSOIL software. Additionally, Bijukchhen *et al.* (2017) highlighted the vulnerability of the Kathmandu Valley to seismic waves, constructing 1D velocity models to reveal the undulating topography and sedimentary deposits of the Valley. Meanwhile Shah (2018) used DEEPSOIL software to conduct the one-dimensional response analysis to analyse the varying earthquake impacts in Gongabu and Balaju highlighting the impact of silty sand and clay soil on earthquake impacts. Thapa and Upadhyaya (2020) examined the vulnerability of indigenous communities in three districts of Nepal i.e. Kailali, Chitwan, and Rautahat to climate change, while Rai *et al.* (2020) focused on assessing climate change vulnerability in Lamjung district, Nepal, considering conceptualization, engagement, and experimentation as parameters of awareness.

Meanwhile, Guragain *et al.* (2020) conducted a 1D ground response analysis through an equivalent-linear analysis approach using Kobe earthquake ground motion with DEEPSOIL software. Carlos *et al.* (2022) addressed the urban risk issue by investigating changing spatial dynamics among natural hazards, expanding urbanization, and social vulnerability in Kathmandu Valley. Bhochhibhoya and Maharjan (2022) carried out a study on vulnerability assessment of seismic hazards at the district level in Nepal, integrating social conditions with hazard-risk analysis to develop an integrated vulnerability score for the regions and presented in the form of maps using ArcGIS. Similarly, the study carried out by Bhusal *et al.* (2022) employed both linear and non-linear techniques using DEEPSOIL software to assess the seismic behaviour, considering the soft soil conditions iden-

tified in borehole logs for the Dharahara monument in Kathmandu, Nepal. Regmi *et al.* (2023) assessed the implementation of a vulnerability and risk assessment framework in Nepal, highlighting the collaborative efforts of the government and stakeholders.

This study fills a significant gap in seismic risk assessment by estimating the vulnerability index to develop a comprehensive seismic vulnerability index map for the Kathmandu Valley, using the Gorkha earthquake as the input motion for enhanced accuracy. It is unlike previous studies, which relied on different seismic events such as the Kobe earthquake, Uttarkashi earthquake, Chamauli earthquake, etc., which are not comparable to the Gorkha earthquake in terms of peak ground acceleration (PGA) due to differences in magnitude, focal depth, epicentre location, fault mechanism, geological conditions, and building practices. Each earthquake event has unique characteristics that influence the intensity and distribution of ground shaking resulting in varying PGA levels. This deliberate choice ensures a more precise representation of seismic hazards specific to the study area. Moreover, by addressing the limitations identified in previous studies, this study makes a substantial contribution to seismic risk analysis. The Gorkha earthquake sparked further interest and investigation into vulnerability assessment, risk reduction, and community resilience building in Nepal, which resulted in advancements in construction codes, emergency preparedness, and the adoption of strategies to boost community resilience.

2. Geology and seismicity

Young fluvial-lacustrine deposits in the Valley can be up to 600 m thick (Mori *et al.* 2020). The two main geological groups that make up the Kathmandu Valley are the Bhimphedi and the Phulchoki Group, both of which are located in the Bagmati Province of the Kathmandu district. The hill terraces used to build it date back to the middle to late Pleistocene. The three main formations in the southern section of the Valley are Tarebhir, Lukundol, and Itaiti. Sediment deposition results from the Bagmati formation, which was active before the formation of lake (Thapa and Guoxin 2013). The black clayey deposits, which are found in the central portion of the Valley, have dark-grey layers with a high carbon and diatom concentration. The Patan Formation lies on the top of the basin. It is made up of clay, fine gravel, and silt with small to medium-sized sand particles dispersed throughout. The northeastern and northern portion of the Valley are composed of the flaviolacustrine Gokarna Formation and Thimi Formation, respectively (Chamlagain and Gautam 2015). In the Valley, there are numerous fault networks that traverse the rocks. The faults that have damaged terraces and other landforms in the southern part of the Valley are the Chovar and Chandragiri faults.

The Himalayas, a prominent example of a seismotectonic structure, are formed when the Indian and Tibetan plates collide. Three main thrusts (i) MFT (Main Frontal Thrust), (ii) MBT (Main Boundary Thrust), and (iii) MCT (Main Central Thrust) affect the main seismic characteristics of the Himalayas, which are thrust faults that move from north to south. The Main Himalayan Thrust, which represents the under thrusting of the Indian tectonic plate beneath the Eurasian Plate, is most frequently thought of as the source of the MFT system, which are splay thrusts. Mudstone is found near the base of the Siwalik rocks that make up the thrust slices that form the MFT structure, and conglomerate and many sandstone strata are found at the top. Crystalline nappes are a common sight in the lower Himalayan region in the western Himalayas. The MBT is currently the most active thrust system, whereas the MCT has been operational for centuries. On the other hand, the MFT is thought to be the newest. The Greater Himalayas are located north of the MCT and between the MCT and the ISZ. They are composed of intrusive rocks with a coarse texture. The Lesser Himalayas are situated south of the MBT and are composed of sedimentary layers that the MBT divides. The Outer Himalayas, which are composed of the layers formed during the Miocene epoch demonstrate the curvature and tectonic faults, are located south of the MBT. Several nations border this mountain range, including Nepal, India, Bhutan, China, and Pakistan.

3. Data and methodology

A total of 135 boreholes location from the Kathmandu district (Anamnagar, Budhanagar, Baneshwor, Bagbazar, Balkhu, Basbari, Chandol, Dhapasi, Ghantaghar, Gahanapokhari, Gurjudhara, Kalopul, Kirtipur, Lainchaur, Mandikatar, Naxal, Pradarsani Marga, Sinamangal, Sundari Jal, Suntol, and Tahachal), 58 boreholes from the Lalitpur district (Balkumari, Bhaisepati, Bhanimandal, Chakupat, Hattiban, Jawalakhel, Khumaltar, Kopundol, Nakhipot, Sanepa, Satdobato, Talchikhel), and 32 boreholes from the Bhaktapur district (Dudhpati, Libali, Manohara, Mulpani, Nagarkot, Ram Mandir, Sanothimi, and Itachhen) are considered for the study. This study, which includes 225 boreholes located at various areas of the Valley as shown in Fig. 1, follows the following working procedure for calculating the vulnerability index (K_g as depicted in Fig. 2).

The foremost step in calculating K_g is the data collection of standard penetration test of soil deposits, determination of shear wave velocity (V_s), dominant frequency (f_o), and amplification factor (A_o). The key factors that contribute to soil amplification include soil type, stiffness, thickness, and geological conditions. Soft, loose, and saturated soils, such as clay, silt, and loose sand, tend to amplify seismic waves more than stiffer soils or bedrock. It has been observed that the collected lithology of the soil deposits of the Valley consists of
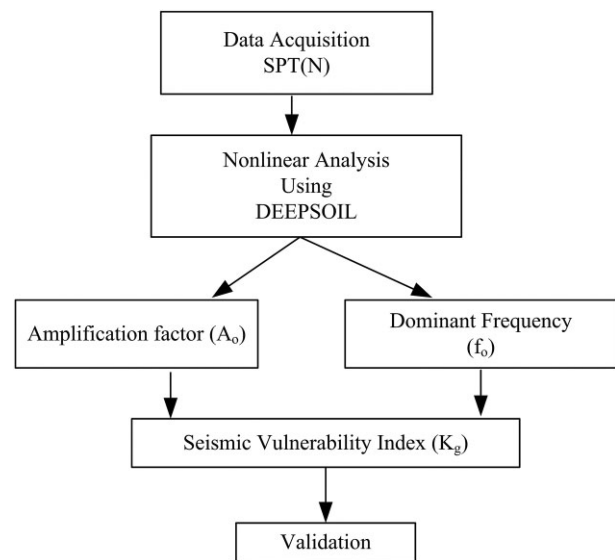

Figure 2. Methodological illustration for vulnerability index.

the layers of medium dense, medium to fine sand, dense to very dense, medium to coarse sand with fine gravels, black silt, and medium dense to dense poorly graded sands etc.

3.1. Shear wave velocity

Shear wave velocity (V_s) is a key parameter in understanding soil amplification, which refers to the increase in ground motion amplitudes experienced in soft or loose soil compared to bedrock conditions. It plays a vital role in assessing site response, calculating site-specific amplification factors, and calculating the fundamental period of the soil layers. Shear wave velocity helps evaluate the possibility of soil amplification and its consequences for structure design by describing the dynamic behaviour of the soil. At first geotechnical data based on laboratory tests conducted in various civil engineering projects at different sites in the Valley is collected. Parameters such as soil classification, unit weight, standard penetration test N value (standard penetration resistance), and shear strength parameters for soils at each site were studied. As there is not enough information available for the Kathmandu Valley to produce highly representative shear wave velocity $V_s - N$ equations. Using N values from various sources, Saifuddin *et al.* (2021) constructed a compilation of 40 empirical equations for calculating shear wave velocity. One study by Gautam (2017b) generated the empirical correlations from secondary sources by combining geological and geotechnical data with lithostratigraphic data. For the top 30 m of the soil column, three equations have been separately constructed for all soil types, silt, and sand. In this study, the established correlation for all soil types as shown in Equation (1) is used, which demonstrates an impressive

Table 1. Classification of soil based on dominant frequency (adopted from Nurwidyanto *et al.* 2023).

Soil classification type	Dominant frequency (Hz)	Kanai's classification
Type IV	<2.5	Alluvial rock with a thickness of 30 mor more, formed by topsoil delta sedimentation, mud, etc.
Type III	2.5–4	Sand gravel, sandy hard clay, loam, etc. make up alluvial rock that is >5 m thick
Type II	4–6.67	Sand gravel, sandy hard clay, loam, etc. that make up the 5-m thick alluvial rock
Type I	6.67–20	Tertiary rocks consisting of sandy hard rocks, gravel, etc.

familiarity with the pre-existing correlations.

$$V_s = 115.8N^{0.251},\qquad(1)$$

where N represents the standard penetration resistance.

3.2. Dominant frequency

To fully evaluate the susceptibility of structures to amplify ground shaking, particularly in regard to soil amplification effects, the f_o must be taken into account in nonlinear response analysis. The dominant frequency, which is intimately related to soil amplification, significantly affects the structural response to earthquakes. The thickness of each layer plays a vital role in a nonlinear analysis since it directly affects the highest frequency that may be transmitted through the soil. Lower maximum frequencies can be transmitted via a layer with a greater thickness than higher maximum frequencies can be transmitted through a layer with a thinner layer. This formula given in Equation (2) expresses the relationship between the maximum frequency and soil thickness.

$$f_o = \frac{V_s}{4H},\qquad(2)$$

where, H stands for the thickness of soil layer, V_s represents the overall shear wave velocity across the entire depth, and f_o the highest possible frequency that can be propagated. In this study, soil classification of the study area based on the dominant frequency has been classified as per Table 1.

3.3. Ground response analysis

Site response analysis can be conducted using various models, including linear, equivalent-linear, or nonlinear models. The linear model presupposes damping at small strains and a constant shear modulus. The equivalent-linear model is a refinement of the linear model and at the same time a straight forward substitute for the nonlinear model. Shear modulus and damping ratio at each shear strain level are iteratively calculated under the assumption of the nonlinear characteristics, and the results are then used to estimate the site response. The shear modulus and damping ratio vary during the loading period in the whole nonlinear analysis at all strain levels. Although frequency and time domains are used for

both linear and equivalent-linear studies, only the time domain is used for nonlinear analysis. The equivalent-linear model becomes erroneous at a shear strain of 0.1%–0.4% but the linear model assumption fails at a shear strain of 0.01%–0.1%. Large strain values (>0.4%) necessitate the use of nonlinear analysis, which also aids in enhancing the outcomes for strains higher than 0.05% (Ansari *et al.* 2023). The nonlinear analysis is most suitable for this study since the greatest shear strain created in the deep and soft deposits of the Valley subjected to substantial intensity levels is typically >0.05%. The 1D nonlinear response analysis is based on the ideas that superficial soil layers extend horizontally across elastic rock and that vertically propagating horizontally polarized waves dominate the seismic ground motion wavefield. Nonlinear response analysis and vulnerability assessment based on soil amplification are significant and feasible to correctly predict how structures will respond to seismic forces by taking into account the properties of soil amplification and frequency content. This integration is essential because it provides a more thorough insight of how structures will actually behave when subjected to increase ground shaking conditions and reveals any potential weak points. The response of structures to seismic occurrences can be captured more precisely when soil amplification is taken into account in the study. The inclusion of soil amplification features aids in accounting for the amplification effects brought on by certain soil conditions, which can have a big impact on the response of the structure. In this study the possible amplification of ground motion that structures may encounter is considered the nonlinear response analysis by taking site-specific amplification factors and frequency content into account using the Newmark β method. This factor must be considered as it allows for a more accurate evaluation of the potential weaknesses and failure mechanisms linked to magnified ground shaking. Some of the well-known programmes used for the nonlinear response analysis are STRATA, DEEPSOIL, SHAKE, and SHAKE91. Among them, DEEPSOIL is used in this study as it has a user-friendly interface, excels in handling complex soil-structure and interaction scenarios, and accurately predicts the response of soil layers and structures under seismic loading. Its extensive validation and verification processes further enhance the credibility and reliability of the results (Hashash *et al.* 2020).

DEEPSOIL software has been employed in various research studies across different fields. Adampira *et al.* (2015) compared the spectrum responses with spectral acceleration in Assaluyeh of Iran while Iswanto and Yee (2016) calculated the surface acceleration at the West Bangka site using DEEP-SOIL. Kim *et al.* (2016) computed the relative differences in spectral accelerations and Fourier amplitudes at Obregon Park in Angeles whereas Mahmood *et al.* (2019) determined the amplification factor and spectral acceleration at Peshawar district of Pakistan, and Yildiz (2021) figured out the spectral acceleration, PGA and lateral displacements in Istanbul using DEEPSOIL software. Similarly, Groholski *et al.* (2016) introduced a new quadratic/hyperbolic model for simplified 1D nonlinear seismic site response analyses using DEEP-SOIL software offering improved Yildiz performance compared to hyperbolic models, emphasizing accurate representation of maximum shear stress at Pacoima Dam. Likewise, Stanko *et al.* (2019) conducted the amplification assessment for Ivanec city using equivalent-linear response analysis with DEEPSOIL software and revealed two distinct microzones within the city: one characterized by significant amplification in the central region, attributed to the soft soil properties, and another displaying minimal amplification. While Tran *et al.* (2021) conducted the ground response analysis at the Ba Dinh square area in Hanoi, Vietnam, focusing on one-dimensional nonlinear and equivalent-linear response analyses using DEEPSOIL software and developed a site model based on *in situ* shear wave velocity profiles and geotechnical data. Jalil *et al.* (2021) focused on assessing the effect of local soil characteristics on modifying one-dimensional linear soil response using DEEPSOIL software in the Balaroa, Petobo, and Jono Oge regions revealing amplification factors with peaks around 1.49, 2.05, and 1.27 times for Balaroa, Petobo, and Jono Oge, respectively.

To characterize the dynamic properties of the soil for site response investigations, it is crucial to choose the proper shear modulus degradation and damping ratio curves with respect to shear strain. Site response analysis frequently uses empirical modulus reduction and damping curves, to depict dynamic soil behaviour in the absence of site-specific data. This formulation is an empirically based modified hyperbolic model to predict the nonlinear dynamic responses of different soil types. In this study, the soil behaviour curves for damping and modulus reduction were represented and fitted using the MRDF method as shown in Fig. 3, which takes into account the confining pressure, the plasticity index (PI), angle of friction (φ) the over consolidation ratio (OCR), the excitation frequency (f), and the number of loading cycles (N). Based on the available soil data for the area, a PI between 3.2% and 36% and φ between 17 and 38° has been used. When calculating reference dynamic curves for the Darendeli (2001) model, the coefficient of earth pressure at rest (K_o) is computed using Equation (3) given by Hashash *et al.*

(2020) and the parameters OCR, N, and f are taken as 1, 10, and 1, respectively, during the analysis (Tran *et al.* 2021):

$$K_o = (1 - \sin\varphi)OCR^{\sin\varphi}. \tag{3}$$

To accurately represent the constitutive behaviour of the soil, the maximum cut-off frequency, f_o of 30 Hz was chosen. To prevent excessive high-frequency wave attenuation, the limit of f_o ensures that the thickness is minimal enough to permit the passage of sufficiently high-frequency waves through the soil deposit. The DEEPSOIL software includes a range of soil models that take into account the depth-dependent behaviour of soils. In this study, the shear modulus and damping ratio curves were fitted to the reference curves using the pressure-dependent modified Kondner–Zelasko model and non-Masing reloading-unloading hysteretic formulation. The nonlinear behaviour of the soil column is captured by the modified Kondner–Zelasko model. It is an extended hyperbolic model with two additional curve fitting parameters, s and β, are used to modify the backbone curve to achieve the proper shear stress and shear strain values. For DEEP-SOIL to mimic seismic loading, input ground motion, i.e. the Gorkha earthquake and the response spectra of PTN station as shown in Fig. 4 is used in this study. The maximum horizontal acceleration at PTN was 0.5, 0.13, and 0.15g for the NS, EW, and vertical components respectively.

The bedrock is defined as a rigid half space. The maximum strain increment is 0.5% and the effective shear strain ratio considered for the analysis is 0.65. The motion equations for the structure and soil layers were then solved using an iterative process. This method provided a more accurate evaluation of the surface spectral acceleration by taking into consideration the stiffness and damping effects brought on by soil-structure interaction. To solve the nonlinear equations of motion and faithfully replicate the dynamic response of the system, step-by-step integration techniques was used. The peak ground spectral acceleration corresponds to the surface spectral acceleration of the soil deposit and is used for the computation of the soil amplification. Based on the classification by (Adib *et al.* 2015) the soil amplification factors in this study are classified into five zones as shown in Table 2.

3.4. Seismic vulnerability index

A quantitative measure that evaluates the susceptibility of buildings and communities to potential harm or failure due to amplified ground shaking brought on by soil amplification effects and the dominant frequency of the seismic waves is the vulnerability index. It establishes the degree of susceptibility of the surface layer vulnerability during seismic activity and is determined by

$$K_g = \frac{A_o{}^2}{f_o}. \tag{4}$$
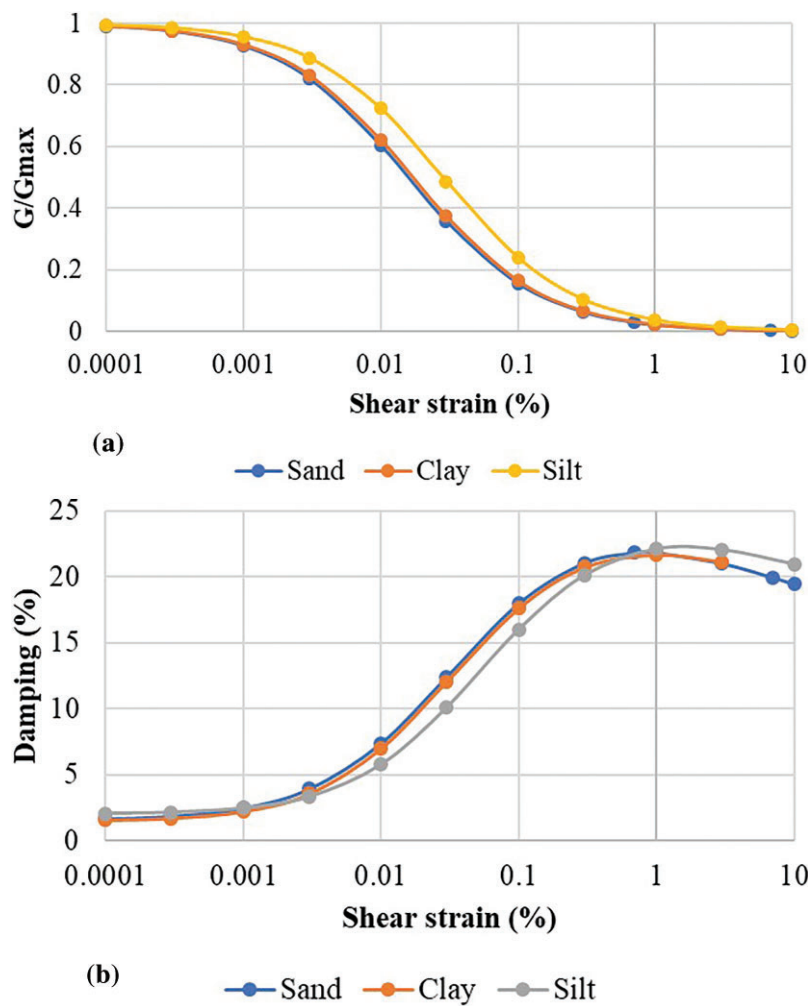
Figure 3. Adopted dynamic properties of the soil: (a) G/G_{max} modulus reduction curve and (b) damping curve with respect to shear strain.

In this study, the risk zone based on vulnerability index has been considered according to Adib *et al.* (2015) and risk level has been categorized into five zones shown in Table 2.

Strong zones that are vulnerable to damage in the case of an earthquake are indicated by areas highlighted with high K_g values. The obtained results were interpolated in ArcGIS using inverse distance weighting considering a processing extent the same as the layer Valley. After that, raster analysis was done with cell size as maximum of inputs and depicted as spatial zonation maps based on V_s, f_o, PGA at surface, A_o, and K_g.

4. Results

In this study, the integration of dominant frequency (f_o) and soil amplification (A_o) obtained is assessed to calculate and identify low- and high-risk zones based on vulnerability index (K_g) of the Kathmandu Valley. High K_g values suggest a weak zone that may sustain damage during an earthquake. The K_g is used to measure seismic vulnerability and defines

the degree of surface layer susceptibility to deformation during seismic events. The findings are discussed in the following sections.

4.1. Shear wave velocity and dominant frequency

The map shown in Fig. 5a provides the variance of shear wave velocity (V_s) of the study area. The V_s is found to be high for the sites with high N value due to the relative stiffness as a result of overburden pressure. It is observed that the velocity increases with depth generally increases while being lower at shallow depths. The calculated shear wave velocity ranges between 150.69 and 306.65 m/s indicating that surface deposits are relatively soft. The dominant frequency (f_o) of the study area varies from 0.08 (Kirtipur) to 7.65 Hz (Gahanapokhari), which shows the significant geological variance. The distribution and soil classification based on f_o in the form of map is shown in Fig. 5b and c.

The results of this study show that higher dominant frequencies in the areas of Hattiban and Gahanapokhari (6.67–
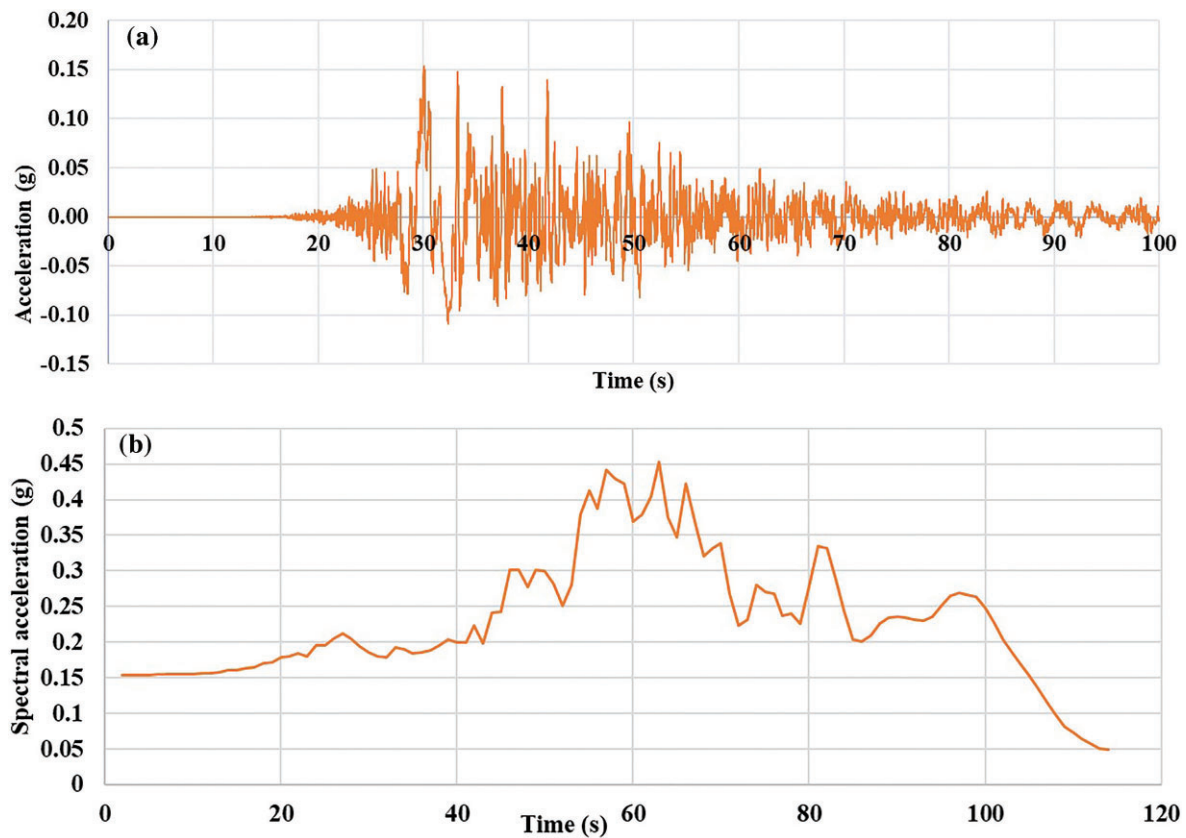
Figure 4. (a) Input motion: the Gorkha earthquake and (b) response spectra of Gorkha earthquake.

Table 2. Zone classification according to A_o and K_g.

| Zone classification	Amplification factor (A_o)	Vulnerability index (K_g)
Very low	<1.6	<1.2
Low	1.6–2.7	1.2–4.2
Medium	2.7–5.4	4.2–10
High	5.4–6	10–19
Very high	6–10	19–40

7.65 Hz, Type I) exhibits the tertiary sandy rock. Locations such as Sinamangal, Basbari, Tahachal, Chandol, Bhaisepati, Balkhu, Nagarkot, Gurjudhara, Thimi, and Itachen of Kathmandu Valley (4–5.78 Hz, Type II) are found to exhibit the thinner and stiffener sediments layer with higher densities and allow the propagation of seismic waves more quickly, while lower dominant frequencies (0.08–2.48 Hz, Type IV) found in Kirtipur, Ghantaghar, Tangal, Khumaltar, Jawalakhel, Mandikatar, Mulpani, Baneshwor, Balkhu, and Bagbazar exhibit thicker layers. Seismic waves need more energy to travel through a thicker sediment layer. As a result, the slower seismic waves due to the higher mass have a lower f_o. In addition, the areas such as Gahanapokhari, Lainchaur, Kopundol, Mandikatar, Balkumari, Sanothimi, Satdobato, Bhanimandal, Kalopul, Sanepa, Libali, Anamnagar,

Pradarsani Marga, and Khumaltar (almost ∼46.23% of the analysed borehole) have the dominant frequencies of type III frequencies ranging from 2.5 to 4 Hz. Similarly, ∼30.67% of analysed borehole has low frequency value ranging from 0.08 to 2.48 Hz i.e. Type IV. In this study ∼19.56% of the analysed boreholes result higher f_o (Type II), which concludes that a thin layer of sediments propagates the seismic wave easily in the Valley. Likewise, ∼3.6% of the analysed boreholes have dominant frequency ranging from 6.67 to 7.65 Hz. When the dominant frequency (f_o) of the sediment layer coincides with the frequency of seismic waves, resonance happens. As a result, the amplification factor increases and so is the vulnerability index.

4.2. Soil amplification and vulnerability index

The surface PGA has been calculated from the nonlinear analysis using DEEPSOIL and mapped as shown in Fig. 5d. In this study it is seen that soil responded more linearly to low-intensity input ground movements of 0.01g greatly delaying stiffness degradation and amplifying bedrock to surface accelerations at the surface of soil layers and the dominant peak frequency. Amplification rapidly diminishes as input ground motion acceleration is increased (0.17g at 0.95 s), which is because large induced stresses greatly reduce stiff-
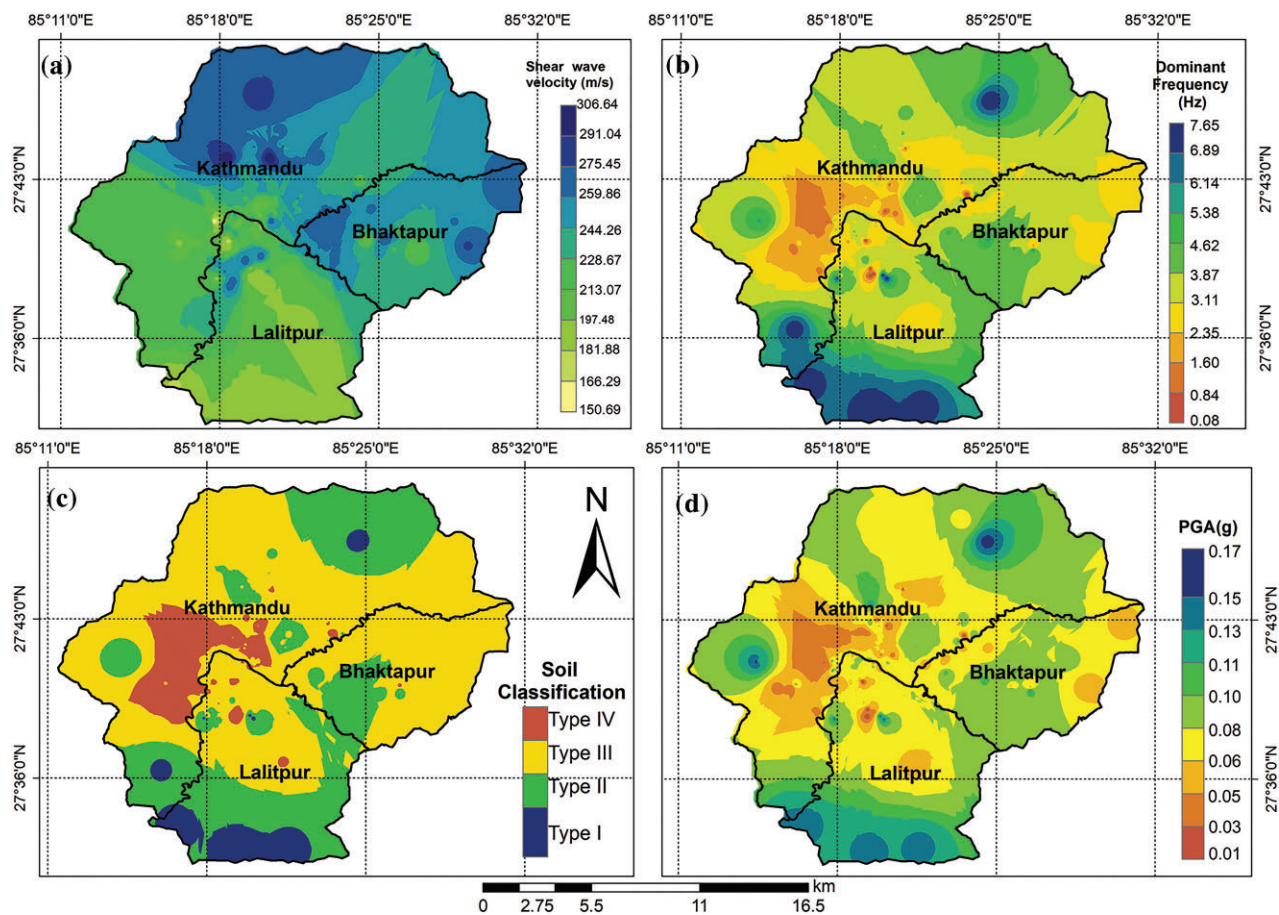
Figure 5. (a) Shear wave velocity map, (b) distribution of dominant frequency, (c) classification of soil according to dominant frequency, and (d) Surface PGA map.

ness and increase hysteretic damping, which decreases the soil ability to transmit force to the overlying surface. When a rock has a PGA >0.17, nonlinear behaviour of the soil is anticipated. The nonlinear soil response causes the induced strain to be increased and the shear modulus (stiffness) to drop at low-to-mid frequencies, which causes the prominent peak to be compressed with greater input intensities. The distributions of soil amplification A_o and vulnerability index (K_g) shown in Fig. 6a and c, suggest that regions with higher soil amplification factor also tend to have higher seismic vulnerability, or vice versa.

In this study the degree of soil amplification ratio of Valley varies from 0.15 (Kirtipur) to 8.14 (Basbari). In Basbari area the surface soil layer consists of filling material including sandy silt and the subsequent layers are made up of silt and sand with low to medium plasticity. At a frequency of 4.3 Hz, the average shear wave velocity for this location has been calculated to be 258.61 m/s and is classified as a very high amplification zone. A higher vulnerability is indicated at this location by the combination of a higher amplification factor of 8.14 and K_g equal to 15.41 and a low predominant period which enhance the damage from earthquakes. The soil

configuration of Bhaisepati, Sinamangal, and Nagarkot are similar with greater amplification ratios ranging from 6.13 to 7.9 as shown in Fig. 6b at a maximum frequency of 4.2 Hz and has been categorized as a very high amplification zone. In the same way, vulnerability indexes (K_g) between 4.28 to 12.12 in Nagarkot (medium to high-risk zone as shown in Fig. 6b) and 1.64 to 15.07 (low to high-risk zone as shown in Fig. 6b) in the Sinmangal area have been observed. The boreholes incorporate the sandy and clayey silt, which has resulted to higher amplification and vulnerability index in these areas and are more likely to experience more ground shaking during earthquakes.

The sites such as Anamnagar, Bakhundol, Balkhu, Balkumari, Bhanimandal, Khumaltar, Kopundol, and Mandikatar have soil amplification factors and K_g ranging from 2.16 to 4.28 and 0.27 to 3.28, respectively, and these areas fall under medium and very low to low-risk zones (Fig. 6b). The type of soil found in these areas contains clayey silt of low to medium plasticity. The soil amplification 2.7 of Kopundol and 1.24 of Tangal area obtained in this study falls under a low amplification zone. As result their vulnerability index (K_g) ranging between 0.57 to 2.08 and 0.57 to 0.71 also
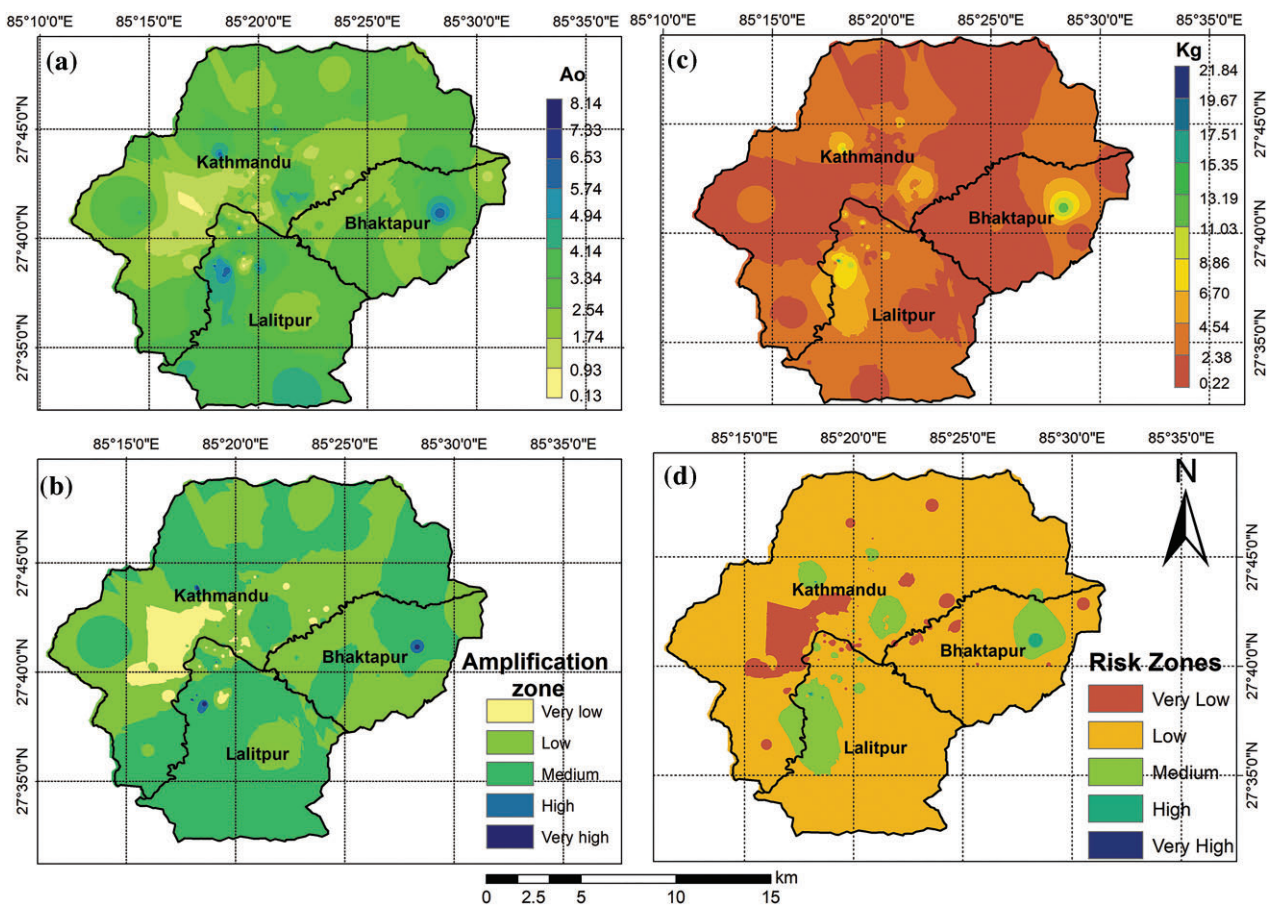
Figure 6. (a) Soil amplification map, (b) soil amplification zone map, (c) vulnerability index map, and (d) risk zone map based on K_g.

falls under the low-risk zone as shown in Fig. 6d. In addition, the soil in the Jawalakhel region has soil amplification of 5.92 at a frequency of 3.78 Hz and the highest spectral acceleration is 0.07g. In the region, shear waves move at an average speed of 242.06 m/s. Geologically, the region is composed of sandy gravel followed by grey to black clayey low plasticity silt. The A_o and K_g ranging from 4.74 to 6.49 and 5.87 to 11, respectively, was found during the analysis of the Bishnumati Khola bridge. They fall under medium to high amplification and medium risk zone.

The boreholes of Dhapasi area are composed of medium dense to dense poorly graded sand followed by very dense poorly graded sand. The A_o and K_g in this area ranges from 1.81 to 3.72 and 1.07 to 3.77, respectively, at a frequency of 3.05 to 5.17 Hz with a shear wave velocity of 228.79 to 266.89 m/s, respectively. A range of 2.59 to 6.12 and 1.64 to 15.07 for the A_o and K_g has been observed (Fig. 6a and c) in well-graded sand with silt in the Sinamangal area. This range represents the potential increase in ground shaking when seismic waves travel through this particular soil type in comparison to the input motion at the bedrock level. The higher end of the range, 6.23 and 15.07, denotes a more prominent amplification effect and may lead to significantly larger ground shaking

in comparison to the input motion at the bedrock level and the area falls under low to high amplification and risk zone.

It has been noted that the soil amplification (A_o) and vulnerability index (K_g) in the Sanepa area ranges from 1.63 to 6.07 and 0.67 to 12.79, respectively. The soil found in this area is stiff to very stiff dark greyish elastic silt. The range of A_o and K_g lying between 63 to 6.07 and 0.67 to 12.79 (low to high amplification and risk zone as shown in Fig. 6b and d) with the maximum frequency of 2.88 Hz in this instance suggests that stiff to very stiff dark greyish elastic silt in this area can have considerable influence on soil amplification. Thus, the variation in soil amplification ratios within the study area suggests the degrees of seismic wave amplification. The soil amplification ratios calculated in Bhaisepati, Jawalakhel, and Sinamangal areas in this study are similar to the study carried out by Chamlagain and Gautam (2015). De-amplification was also observed in locations such as Tangal, Kirtipur, Pradarsani Marga, Bhanimandal, Khumaltar, Mulpani, and Balkhu area with an amplification and vulnerability index ranging from 0.13 to 0.8 and 0.22 to 3.2, respectively; as a result, these locations have been categorized as very low amplification and low-risk zones as shown in Fig. 6b and d.

Similarly, the calculated values of the vulnerability (K_g), ranging from 0.22 to 21.84 represent the relative vulnerability of different locations within the study area. A K_g value of 0.22 at Kirtipur indicates a relatively lower vulnerability, suggesting that the area is less susceptible to seismic hazards and may experience less damage during an earthquake. On the other hand, a K_g value of 21.84 at Bhaisepati represents a higher vulnerability, indicating that the area is more prone to strong ground motion and potential damage. As K_g is directly proportional to square of soil amplification, the area as discussed previously having a higher amplification will have a higher K_g, which increases the likelihood of structural damage. This suggests that regions with greater soil amplification factors and K_g also frequently have greater seismic risk, or vice versa. The light green, dark green, and blue highlighted areas are the medium-, high-, and very high-risk zones based on K_g, respectively.

The results in locations such as Anamnagar, Bakhundol, Bhanimandal, Pradarsani Marga, Chakupat, Hattiban, Khumaltar, Kirtipur, Kopundol, Mandikatar, Mulpani, Sinamangal, Ram Mandir Bhaktapur, Thimi, Lainchaur, Itachen, Naxal, New Baneshwor, Balkhu, Bagbazar, Ghantaghar, Kalopul, Lainchaur, Buddhanagar, Chandol, Ghanapokhari, Gurjudhara, Libali, Lainchaur, Tahachal, Nagarkot, Nakhipot, and Telecom office Bhaktapur have K_g ranging from 0.22 to 4.02 and fall under very low to low-risk zones (Fig. 6b and d). Likewise, the areas Satdobato, Bal Kumari, Bhainsepati, and Pradarsani Marga have low to medium K_g ranging from 1.72 to 10.29, and are considered as being in the low to medium risk zone. A medium amplification and risk zone shown in Fig. 6b and d ranging from 3.91 to 4.21 and 6.29 to 8.55 is observed in Talchikhel area. Similarly, a very low to high-risk zone was found in Sanepa and Basbari area. A vulnerability index (K_g) lying between 1.64 and 15.07 in the Sinmangal area has been considered in the low to high-risk zone. The Jawalakhel area has a K_g lying between 1.04 and 9.27 is considered as being in the very low to medium risk zone. When the f_o is low and the A_o is high, it results in a high K_g indicating that the area has a high risk of earthquake damage, as opposed to an area with a low K_g and a high f_o and low amplification factor. This suggests that regions with greater A_o and K_g also frequently have greater seismic risk, or vice versa.

5. Discussion

5.1. Shear wave velocity and dominant frequency

These V_s results are also justified by the study carried by Goda *et al.* (2015). The NBC 105 (2020) categorized the types of soil as types A through D, ranging from very hard to soft soil. In accordance with the NBC 105:2020, the Kathmandu Valley has category D soil, which is exceptionally soft soil. Additionally, the type of soil found in the study area is

type D, and is also justified by the result of the study. The amplification and transmission of seismic waves are influenced by the shear wave velocity of the subsurface materials. Ground shaking is more likely to be amplified at certain frequencies in softer, less-consolidated materials with lower shear wave velocity of 150.69 m/s. On the other hand, less amplification may result from stiffer materials with a higher shear wave velocity of 306.65 m/s. This indicates that the subsurface geology has a different type of soil and rocks, layer thickness, and stiffness. As a result, seismic waves behave differently and causes changes in the main frequency values. The thickness of a sediment layer has an inverse relationship with the dominant frequency f_o as a result; thinner layers typically have higher dominant frequencies than thicker layers, who tend to have lower dominant frequencies (Sorja *et al.* 2019).

The different seismic profiles of these regions suggest the potential existence of certain geological features or tectonic processes that affect the formation of seismic waves in this frequency range. The improved seismic wave propagation at these frequencies raises the likelihood of considerably stronger subsurface structures or geological formations that could affect the seismic behaviour in these areas. Owing to the predominance of these higher dominant frequencies, seismic events that originate in these regions may exhibit distinctive characteristics. The Tri Chandra campus, Ghantaghar one of the oldest campuses of Nepal is currently being retrofitted. The campus buildings sustained damage as a result of the 2015 Gorkha earthquake. The campus was founded in 1918, under Rana Prime Minister Chandra Shamsher, and had already been hit by two significant earthquakes in 1934 and 2015. Similarly, the quake had less of an impact on the Kirtipur neighbourhood, which is thought to be built on a solid foundation. Owing to its distinctive geology, this region has a history of enduring earthquakes, notably the one that struck in 1934 (Maharjan *et al.* 2019). Hence softer and less-consolidated materials with lower shear wave velocities tend to amplify ground shaking at specific frequencies. By contrast, stiffer materials with higher shear wave velocities can lead to less amplification.

5.2. Soil amplification and vulnerability index

Severe destruction was observed during 2015 Gorkha along the Bagmati River and its tributaries, including the Bishnumati River and the Manhart River, making those areas more susceptible to seismic loading. Poorly graded sand typically has a very consistent particle size distribution, which can result in greater stiffness and shear strength compared to more granular or fine-grained soils and this is the reason why the soil amplification is less in this area. The same result is justified from this study and the Dhapasi

area is categorized as being in a very low to low amplification and risk zone. Infill masonry walls and other non-structural components were damaged in several high-rise apartment structures in the Kathmandu Valley during the 2015 Nepal earthquake. The structural components only sustained minimal damage. None of the residential complexes had collapsed. After seismic retrofitting, nearly all high-rise units are liveable. Boreholes of the Park View Horizon Apartment in Dhapasi, Kathmandu, has been considered in this study. Similarly, the soil amplification 2.7 of Kopundol and 1.24 of Tangal area obtained in this study matches with the study carried out by Guragain *et al.* (2020).

Previous studies have emphasized the liquefaction susceptibility at numerous areas in the Valley. The liquefaction caused by the Gorkha earthquake, in contrast to past large earthquakes, appears to be very localized and confined. This might be explained by the earthquake's modest ground motion amplitude and low ground water table. Hattiban, Mulpani, and Duwakot are the locations where liquefaction has been reported (Sharma *et al.* 2019). Freshly expelled sand was driven out of an overly pressurized ground surface, creating sand boils. More information about the liquefaction brought on by the 2015 Gorkha earthquake is provided by Sharma *et al.* (2019) and Subedi and Acharya (2022).

A previous study by Gautam and Chamlagain (2016) likewise calculated significant local amplification and substantial variance in motion parameters within the soft soil deposits. The study also revealed that in areas with soft soils, such as Thimi and Bhaktapur as opposed to the southern part of the Kathmandu Valley, local amplification and soil nonlinearity were the main sources of significant damage. Since the 1255 earthquake, Bhaktapur has been the place most severely damaged, while Thimi consistently experiences damage scenarios similar to those of Bhaktapur.

When developing infrastructure around the Kathmandu Valley, the Fig. 6c seismic vulnerability index map and risk zone can be used as a guide. It must be taken into consideration when developing infrastructure for areas with a high seismic K_g value, which have a high level of earthquake damage, that areas with a low K_g have better infrastructure for building economic commodities and public facilities. Thus, the silty facies of clay and increased shear wave velocity are the main regulating reasons for the higher A_o and K_g. Additionally, it has been noted that locations with sandy silt and silty clay have produced the higher A_o and K_g. Regions with a higher vulnerability index, such as those with lower dominant frequencies and higher soil amplification factors, are more susceptible to structural damage and pose a greater risk during seismic events. These findings emphasize the need for targeted interventions, including resilient building codes and infrastructure development, particularly in high-risk zones identified based on vulnerability indices. By prioritizing mitigation efforts in these areas, policymakers can enhance the seismic resilience of the community and reduce the potential impact of future earthquakes.

6. Conclusions

In this study, the estimation of the vulnerability index (K_g) is conducted using the dominant frequency (f_o) and soil amplification (A_o) as key parameters. This study aimed to address the seismic K_g of the Kathmandu Valley. The comprehensive analysis of 225 boreholes using DEEPSOIL software, the f_o and A_o values were ascertained. These variables gave the important information about the soil-structure system and its seismic wave response properties. The dominant frequency values ranged from 0.08 to 7.65 Hz while the amplification factor values ranged from 0.15 to 8.14. These wide-ranging figures demonstrate the geographical variability in soil characteristics and their impact on the seismic response in the Valley. The K_g values ranged from 0.22 to 21.84, with higher values indicating areas at higher risk of significant damage during earthquakes. The integration of microzonation data, nonlinear analysis, and GIS mapping in this study provides a comprehensive approach to assessing and quantifying seismic vulnerability. By delineating the spatial variations in the f_o, A_o, and K_g, the urban planner, land-use management, and policy-making can use this as a valuable tool in reducing the potential impacts of earthquakes on both human lives and the economy. Retrofitting of existing buildings with steel braces, concrete walls, or shear walls, implementing base isolation techniques, improving foundation design, and using flexible materials such as lightweight steel frames and reinforced concrete can enhance seismic resilience. Adopting resilient design standards, building codes, and community education programmes can also promote earthquake-resistant practices and safety measures.

Acknowledgements

Conflict of interest statement: None declared.

Data availability

The data underlying this article will be shared on reasonable request to the corresponding author.

References

Adampira M, Alielahi H, Panji M *et al.* Comparison of equivalent linear and nonlinear methods in seismic analysis of liquefiable site response

due to near-fault incident waves: a case study. *Arabian J Geosci* 2015;**8**: 3103–18. https://doi.org/10.1007/s12517-014-1399-6

Adib A, Afzal P, Heydarzadeh K. Site effect classification based on microtremor data analysis using a concentration-area fractal model. *Nonlinear Proc Geophys* 2015;**22**:53–63. https://doi.org/10.5194/npg-22-53-2015

Aksha SK, Juran L, Resler LM *et al.* An analysis of social vulnerability to natural hazards in Nepal using a modified social vulnerability index. *Int J Disaster Risk Sci* 2019;**10**:103–16. https://doi.org/10.1007/s13753-018-0192-7

Agrawal N, Gupta L, Dixit J *et al.* Seismic risk assessment for the North Eastern Region of India by integrating seismic hazard and social vulnerability. *Sustain Resilient Infrastruct* 2023;**8**:102–32. https://doi.org/10.1080/23789689.2022.2133764

Amirudin, Madrinovella I, Sofian. Seismic vulnerability analysis using the horizontal to vertical spectral ratio (HVSR) method on the West Palu Bay Coastline. *J Geosci Eng Environ Technol* 2023;**8**:23–34. https://doi.org/10.25299/jgeet.2023.8.02-2.13879

Anhorn J, Lennartz T, Nüsser M. Rapid urban growth and earthquake risk in Musikot, Mid-western hills, Nepal. *Erdkunde* 2015;**69**:307–25. https://doi.org/10.3112/erdkunde.2015.04.02

Ansari A, Zahoor F, Rao KS *et al.* Seismic response and vulnerability evaluation of Jammu Region (Jammu and Kashmir). *Indian Geotech J* 2023;**53**:509–22. https://doi.org/10.1007/s40098-022-00694-0

Asnawi Y, Simanjuntak A, Muksin U *et al.* Soil classification in a seismically active environment based on join analysis of seismic parameters. *Glob J Environ Sci Manag* 2022;**8**:297–314. https://doi.org/10.22034/gjesm.2022.03.01

Bhattarai K, Conway D. Urban vulnerabilities in the Kathmandu Valley, Nepal: visualizations of human/hazard interactions. *J Geograph Info Syst* 2010;**02**:63–84. https://doi.org/10.4236/jgis.2010.22012

Bhochhibhoya S, Maharjan R. Integrated seismic risk assessment in Nepal. *Nat Haz Earth Syst Sci* 2022;**2015**:1–28. https://doi.org/https://doi.org/10.5194/nhess-2021-354

Bhusal B, Aaqib M, Paudel S *et al.* Site specific seismic hazard analysis of monumental site Dharahara, Kathmandu, Nepal. *Geomat Nat Haz Risk* 2022;**13**:2674–96. https://doi.org/10.1080/19475705.2022.2130109

Bijukchhen SM, Takai N, Shigefuji M *et al.* Estimation of 1-D velocity models beneath strong-motion observation sites in the Kathmandu Valley using strong-motion records from moderate-sized earthquakes. *Earth Planets Space* 2017;**69**:1–16. https://doi.org/10.1186/s40623-017-0685-4

Carlos M, Cremen G, Galasso C. Urban growth modelling and social vulnerability assessment for a hazardous Kathmandu Valley. *Sci Rep* 2022;**12**:1–16. https://doi.org/10.1038/s41598-022-09347-x

Chamlagain D, Gautam D. *Seismic Hazard in the Himalayan Intermontane Basins: An Example from Kathmandu Valley, Nepal* 2015. https://doi.org/10.1007/978-4-431-55242-0_5

Gautam D. Assessment of social vulnerability to natural hazards in Nepal. *Nat Haz Earth Syst Sci* 2017a;**17**:1–14. https://doi.org/10.5194/nhess-17-2313-2017

Gautam D. Empirical correlation between uncorrected standard penetration resistance (N) and shear wave velocity (VS) for Kathmandu Valley, Nepal. *Geomat Nat Haz Risk* 2017b;**8**:496–508. https://doi.org/10.1080/19475705.2016.1243588

Gautam D, Chamlagain D. Preliminary assessment of seismic site effects in the fluvio-lacustrine sediments of Kathmandu valley, Nepal. *Nat Haz* 2016;**81**:1745–69. https://doi.org/10.1007/s11069-016-2154-y

Goda K, Kiyota T, Pokhrel RM *et al.* The 2015 Gorkha Nepal earthquake: Insights from earthquake damage survey. *Frontiers in Built Environment* 2015;**1**:1–15. https://doi.org/10.3389/fbuil.2015.00008

Groholski DR, Hashash YMA, Kim B *et al.* Simplified model for small-strain nonlinearity and strength in 1D seismic site response analysis. *J Geotech Geoenviron Eng* 2016;**142**:1–14. https://doi.org/10.1061/(asce)gt.1943-5606.0001496

Guragain S, Gautam S, Pokharel K *et al.* Soil amplification factor zonation of Kathmandu Valley. In: *Proceedings of 8th IOE Graduate Conference* 2020;**8**:761–7.

Hashash YMA, Musgrove M, Harmon J *et al. Deepsoil 7* (pp. 1–170). 2020. Urbana, IL, USA, Board of Trustees of University of Illinois at Urbana-Champaign. DEEPSOIL.

Iswanto ER, Yee E. Comparison of equivalent linear and non linear methods on ground response analysis: case study at West Bangka site. *Jurnal Pengembangan Energi Nuklir* 2016;**18**:23. https://doi.org/10.17146/jpen.2016.18.1.2994

Jalil A, Fathani TF, Satyarno I *et al.* Equivalent-linear seismic ground response analysis in Palu area. *IOP Conference Series: Earth and Environmental Science* 2021;**930**:1–3. https://doi.org/10.1088/1755-1315/930/1/012089

Kim B, Hashash YMA, Stewart JP *et al.* Relative differences between non-linear and equivalent-linear 1-D site response analyses. *Earthquake Spectra* 2016;**32**:1845–65. https://doi.org/10.1193/051215EQS068M

Legowo B, Lazuardian RA, Koesuma S. Microzonation of the seismic vulnerability index by using the horizontal to vertical spectral ratio in Boyolali, Central Java. *AIP Conference Procedings 2202,020130(2019)* 2019; *December 2019* 020130–5. https://doi.org/https://doi.org/10.1063/1.5141743

Maharjan SK, Maharjan KL, Dangol DR. Local level socio-economic impacts and responses to the earthquakes-2015: a case of Kirtipur Municipality. *Int J Soc Sci Manag* 2019;**6**:17–27. https://doi.org/10.3126/ijssm.v6i1.22563

Mahbubur RM, Jerin T. Social vulnerability to earthquake disaster: insights from the people of 48th ward of Dhaka South City, Bangladesh. *Environ Hazards* 2022; *June* 1–20. https://doi.org/10.1080/17477891.2022.2085075

Mahmood K, Iqbal Q, Khan H. One dimensional non-linear ground response analysis-a site specific case study of Peshawar District, Pakistan. *Technical J, Univ Eng Technol (UET) Taxila, Pakistan* 2019;**24**:11–8.

Mori T, Shigefuji M, Bijukchhen S *et al.* Ground motion prediction equation for the Kathmandu Valley, Nepal based on strong motion records during the 2015 Gorkha Nepal earthquake sequence. *Soil Dyn Earthquake Eng* 2020;**135**:106208. https://doi.org/10.1016/J.SOILDYN.2020.106208

Mubin F, Nurcahya BE. Frequency analysis and seismic vulnerability index by using Nakamura methods for microzonation at Prambanan Temple and its surrounding area, Yogyakarta Province, Indonesia. *2014 International Conference on Physics, ICP 2014* 2014; *ICP 2014* 91–6. https://doi.org/10.2991/icp-14.2014.18

Nurwidyanto MI, Zainuri M, Wirasatriya A *et al.* Microzonation for earthquake hazards with HVSR microtremor method in the coastal areas of Semarang, Indonesia. *Geographia Technica* 2023;**18**:177–88. https://doi.org/10.21163/GT

Rai K, Neupane BK, Pariyar RK. Climate change vulnerability assessment in the High Mountain Region of Nepal: a case study of Lamjung District. *Int J Environ Clim Change* 2020;**10**:48–59. https://doi.org/10.9734/ijecc/2020/v10i330187

Regmi BR, Sapkota R, Paudyal A *et al.* Co-development of vulnerability and risk assessment framework and methodology for Nepal. *Environ Monit Assess* 2023;**195**:1–17. https://doi.org/10.1007/s10661-023-11330-6

Saifuddin, Sungkono, Widodo A. S-wave velocity (Vs) model uncertainty derived from multiple equations of V_s and number of blows (N) at Institut Teknologi Sepuluh Nopember, Surabaya, Indonesia. *J Phys Conf*

Ser 2021;**1951**:012050. https://doi.org/10.1088/1742-6596/1951/1/012050

Shah S. Site effects of soft soil deposit on ground motion in Kathmandu valley. *1st KEC Conference Proceedings* 2018;**I**:39–42. https://doi.org/10.13140/RG.2.2.15646.38724

Sharma K, Deng L, Khadka D. Reconnaissance of liquefaction case studies in 2015 Gorkha (Nepal) earthquake and assessment of liquefaction susceptibility. *Int J Geotech Eng* 2019;**13**:326–38. https://doi.org/10.1080/19386362.2017.1350338

Sorja K, Putera M, Darsono D. A microtremor analysis for microzonation of seismic vulnerability index by using horizontal to vertical spectral ratio in the southern area of Klaten regency. *J Phys Conf Ser* 2019;**1153**:1–6. https://doi.org/10.1088/1742-6596/1153/1/012023

Stanko D, Markušić S, Gazdek M *et al.* Assessment of the seismic site amplification in the city of Ivanic (NW part of Croatia) using the microtremor HVSR method and equivalent-linear site response analysis. *Geosciences* 2019;**9**:312. https://doi.org/10.3390/geosciences9070312

Subedi M, Acharya IP. Liquefaction hazard assessment and ground failure probability analysis in the Kathmandu Valley of Nepal. *Geoenviron Disasters* 2022;**9**:1–17. https://doi.org/10.1186/s40677-021-00203-0

Sunaryo. Study of seismic vulnerability index (K_g) from dominant frequency (f0) and amplification factor (A0) by means of microzonation data:: case study on Batubesi Dam of Nuha, East Luwu, South Sulawesi, Indonesia. In: *Proceedings of the 2017 International Seminar on Sensors, Instrumentation, Measurement and Metrology (ISSIMM)* 2017;**2017-Janua**:78–81. https://doi.org/10.1109/ISSIMM.2017.8124266

Tallett-Williams S, Gosh B, Wilkinson S *et al.* Site amplification in the Kathmandu Valley during the 2015 M7.6 Gorkha, Nepal earthquake. *Bull Earthquake Eng* 2016;**14**:3301–15. https://doi.org/10.1007/s10518-016-0003-8

Thapa DR, Guoxin W. Probabilistic seismic hazard analysis in Nepal. *Earthq Eng Eng Vib* 2013;**12**:577–86. https://doi.org/10.1007/s11803-013-0191-z

Thapa P, Upadhyaya PS. *Vulnerability assessment of indigenous communities to climate change In Nepal*. 2020;**1**:1–7.

Thapa PK, Baral S. Community-based vulnerability assessment and risk mapping for adaptation planning in Terai eco-zone, Nepal. *J Agric Environ* 2013;**14**:1–12. https://doi.org/10.3126/aej.v14i0.19781

Tran NL, Aaqib M, Nguyen BP *et al.* Evaluation of seismic site amplification using 1D site response analyses at Ba Dinh Square Area, Vietnam. *Adv Civ Eng* 2021:1–11. https://doi.org/10.1155/2021/3919281

Yildiz Ö. Nonlinear and equivalent linear site response analysis of Istanbul soils. *NATURENGS* 2021;**1**:88–101. https://doi.org/10.46572/naturengs.895283

Zhu J, Zhang Y, Zhang J *et al.* Multi-criteria seismic risk assessment based on combined weight-TOPSIS model and CF-logistic regression model—a case study of Songyuan City, China. *Sustainability* 2023;**15**:1–28. https://doi.org/10.3390/su151411216. (in Chinese)